Available online at www.sciencedirect.com
ScienceDirect
Solid-State Electronics 50 (2006) 1732–1739
SOLID-STATE ELECTRONICS
www.elsevier.com/locate/sse

A numerical Schrödinger–Poisson solver for radially symmetric nanowire core–shell structures

Lingquan Wang *, Deli Wang, Peter M. Asbeck

Department of Electrical and Computer Engineering, University of California, San Diego, 9500 Gilman Drive CallT2 Building, La Jolla, CA 92093, United States

Received 4 April 2006; accepted 21 September 2006
Available online 9 November 2006

The review of this paper was arranged by Prof. Y. Arakawa

Abstract

We present here a general purpose numerical Schrödinger–Poisson solver for radially symmetric nanowire core–shell structures for electronic and optoelectronic applications. The solver provides self-consistent solutions of the Schrödinger equation and the Poisson equation in cylindrical coordinates, for nanowire core–shell structures with radial compositional variation. Quantized energy levels as well as their associated electron wavefunctions and populations can be obtained from the solutions. Individual equation solvers were verified by comparison with scenarios where analytical results exist; verification of the self-consistent solution process was done by comparing results in the large radius limit with numerical solutions for a rectangular slab structure. We apply this solver to compute the charge/capacitance–voltage characteristics for a nanowire field effect device with wrap-around gate. It is shown that quantum confinement and the low dimensionality can give rise to, for representative nanowire FETs considered, ~30% reduction in gate capacitance compared to the classically predicted value, and is ~1/3 of the geometrical barrier limited capacitance.

Keywords: Nanowire; Core–shell structure; Self-consistent calculation; Quantum capacitance

1. Introduction

The rapid advancement in semiconductor nanowire growth technology has motivated numerous research efforts aimed at different applications of nanowires in electronics, optics and biology [1–4]. Among various structures under investigation, the nanowire core–shell structure (with a radial variation in material characteristics, such as semiconductor composition) has been very popular, since it provides great versatility for use in devices such as field-effect transistors [5,6], photoemitters and photodetectors. To exploit the unique traits stemming from the 1-D quantum structure of nanowires, systematic understanding of the electrical and optical properties are important. In general, the determination of the electronic energy levels and potential distribution requires the self-consistent solution of the Schrödinger equation and the Poisson equation under cylindrical coordinates. Previous work has shown that a general-purpose self-consistent Schrödinger–Poisson solver can be formulated for Cartesian coordinates (as needed for representative planar epitaxial structures) [7]. This paper reports on a numerical solver and its applications for nanowires, exploiting cylindrical symmetry.

The numerical Schrödinger Poisson self-consistent solver accounts for quantum confinement as well as the 1-D nature of the density of states in nanowires. The structure considered and its associated coordinate system are illustrated in Fig. 1. The solver is generally applicable to nanowires structures with arbitrary material and doping dependence in the radial direction (the core–shell structure

* Corresponding author. Tel.: +1 858 822 6943; fax: +1 858 534 2486.
E-mail address: liw001@ucsd.edu (L. Wang).

0038-1101/$ - see front matter © 2006 Elsevier Ltd. All rights reserved.
doi:10.1016/j.sse.2006.09.013

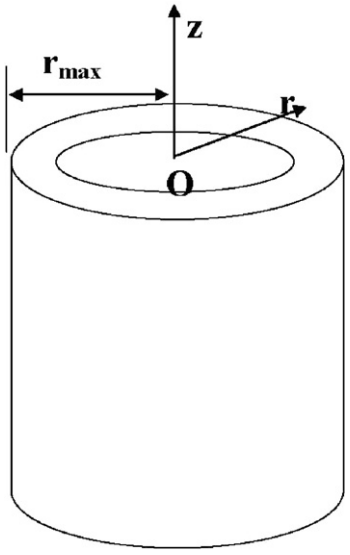

Fig. 1. Schematic of the core–shell nanowire structure and the coordinate system used.

pictured in Fig. 1 has one change in material composition along the radius). The solver uses the conventional finite-difference method to solve the Schrödinger equation. This implies tradeoffs of solution accuracy and computation complexity; values chosen in this work provide reasonable computational times for nanowires of physical interest ($R \sim 5$–500 nm).

From the self-consistent solution, the potential profile, wave functions, electron density and further information can be derived. As an example, the paper illustrates the analysis of capacitance–voltage characteristics for a nanowire core–shell structure configured as an FET, with a radial-deposited metallic gate. For the example case shown in the paper, the gate capacitance is reduced to $\sim 1/3$ of the geometrical barrier limited value, and is only $\sim 70\%$ of the classically predicted value (for which only the Poisson equation is solved).

The paper is organized in the following manner. Governing equations are discussed in Section 2, with emphasis on comparing solutions with cylindrical coordinates and Cartesian coordinates. In Section 3, the solver is tested for a cylindrical constant potential well (where the exact wave functions are known in analytical form) and a core–shell structure with large dimensions (which asymptotically approaches the slab quantum-well solution). The latter result was compared with the solution given by a well-established one-dimensional solver [7] for validation. Section 4 gives an example application of the solver in which a core–shell nanowire structure with metallic gate is characterized in terms of electron distribution and quasi-static C–V characteristics; and mechanisms that cause the gate capacitance reduction are analyzed and de-embedded. Model limitations are briefly discussed in Section 5, while a summary of the paper is provided in Section 6.

2. Schrödinger and Poisson equation solvers

2.1. Schrödinger solver

In the presence of varying material composition, the corresponding spatially-varying effective masses have to be taken into account in the Schrödinger equation. The following form of the Schrödinger equation results:

$$-\frac{\hbar^2}{4}\left[\nabla^2\left(\frac{\Psi}{m^*}\right)+\frac{1}{m^*}\nabla^2\Psi\right]+V\Psi=E\Psi \tag{1}$$

The effective masses are taken to be energy-independent (thus non-parabolicity effects are neglected). We apply the separation of variables method by assuming the overall wave function can be written as

$$\Psi(r,\theta)=R(r)\Theta(\theta) \tag{2}$$

The angular part of the wave function has rotational symmetry, which leads to a solution as

$$\Theta(\theta)=\mathrm{e}^{iv\theta} \text{ with boundary condition :}$$
$$\Theta(\theta+2n\pi)=\Theta(\theta) \Rightarrow v \text{ is an integer} \tag{3}$$

The radial part of the wave function satisfies

$$-\left[\frac{\hbar^2}{2m^*(r)}\left(\frac{\mathrm{d}^2}{\mathrm{d}r^2}+\frac{1}{r}\frac{\mathrm{d}}{\mathrm{d}r}-\frac{v^2}{r^2}\right)+\frac{\hbar^2}{2}\frac{\mathrm{d}\frac{1}{m^*}}{\mathrm{d}r}\frac{\mathrm{d}}{\mathrm{d}r}+\frac{\hbar^2}{4}\frac{\mathrm{d}^2\frac{1}{m^*}}{\mathrm{d}r^2}+\frac{\hbar^2}{4}\frac{1}{r}\frac{\mathrm{d}\frac{1}{m^*}}{\mathrm{d}r}\right]R+V(r)R=ER \tag{4}$$

It may be noted that in cylindrical coordinates, unlike the Cartesian coordinate counterparts, there are additional terms associated with r^{-n} which bring in a singularity at $r=0$. It is therefore necessary to give particular attention to the behavior of solutions in the neighborhood of the origin. Typical nanowire potentials vary slowly around the $r=0$ point, and can therefore be treated as constants when determining the asymptotic solution. As a result, the Schrödinger equation assumes the following form around $r=0$:

$$-\left[\frac{\hbar^2}{2m^*(r)}\left(\frac{\mathrm{d}^2}{\mathrm{d}r^2}+\frac{1}{r}\frac{\mathrm{d}}{\mathrm{d}r}-\frac{v^2}{r^2}\right)\right]R=ER \tag{5}$$

Solutions to the above equation are J-type Bessel functions with integer orders [8], which can be expressed as an infinite polynomial series summation, with v as the order of the Bessel function

$$J_v=\sum_{l=0}^{\infty}\frac{(-1)^l}{2^{2l+v}l!(v+l)!}x^{2l+v} \tag{6}$$

from which the effect of the Hamiltonian operator can be determined at $r=0$

$$\hat{H}J_v|_{r\to 0}=\begin{cases}-\dfrac{\hbar^2}{2m^*}\dfrac{\mathrm{d}^2}{\mathrm{d}r^2}J_0 & v=0\\ -J_v & \text{otherwise}\end{cases} \tag{7}$$

With the knowledge of the Hamiltonian's behavior near the origin, discretization of the Hamiltonian elsewhere is straightforward. The boundary condition implemented in the solver enforces that the wave function goes to zero at the outer shell of the cylinder (i.e. an infinite potential is assumed confining the electrons to the nanowire). Solving for eigenvalues and eigenfunctions of the Hamiltonian matrix yields subband energies and corresponding wave functions. The electron concentration is further calculated with the following:

$$n = \sum_n |\Psi_n(r)|^2 \int_{E_n}^{\infty} f(E)g(E)\,\mathrm{d}E$$
$$g(E) = \frac{1}{\hbar\pi}\sqrt{\frac{2m^*}{(E-E_n)}} \tag{8}$$

where $g(E)$ is the 1-D density of states, and $f(E)$ is the Fermi–Dirac distribution. The summation over subband indices accounts for contributions from all possible subbands, while the integration accounts for contributions belonging to a specific subband (and varying wavevector along the nanowire).

2.2. Poisson solver

Two Poisson solvers are implemented in the overall self-consistent scheme. The first gives a Poisson solution for classical electron distributions only, in conjunction with the Fermi–Dirac distribution. The result is then fed into the Schrödinger solver as an initial guess of the potential profile. The second Poisson solver calculates the potential distribution with the knowledge of electron concentration

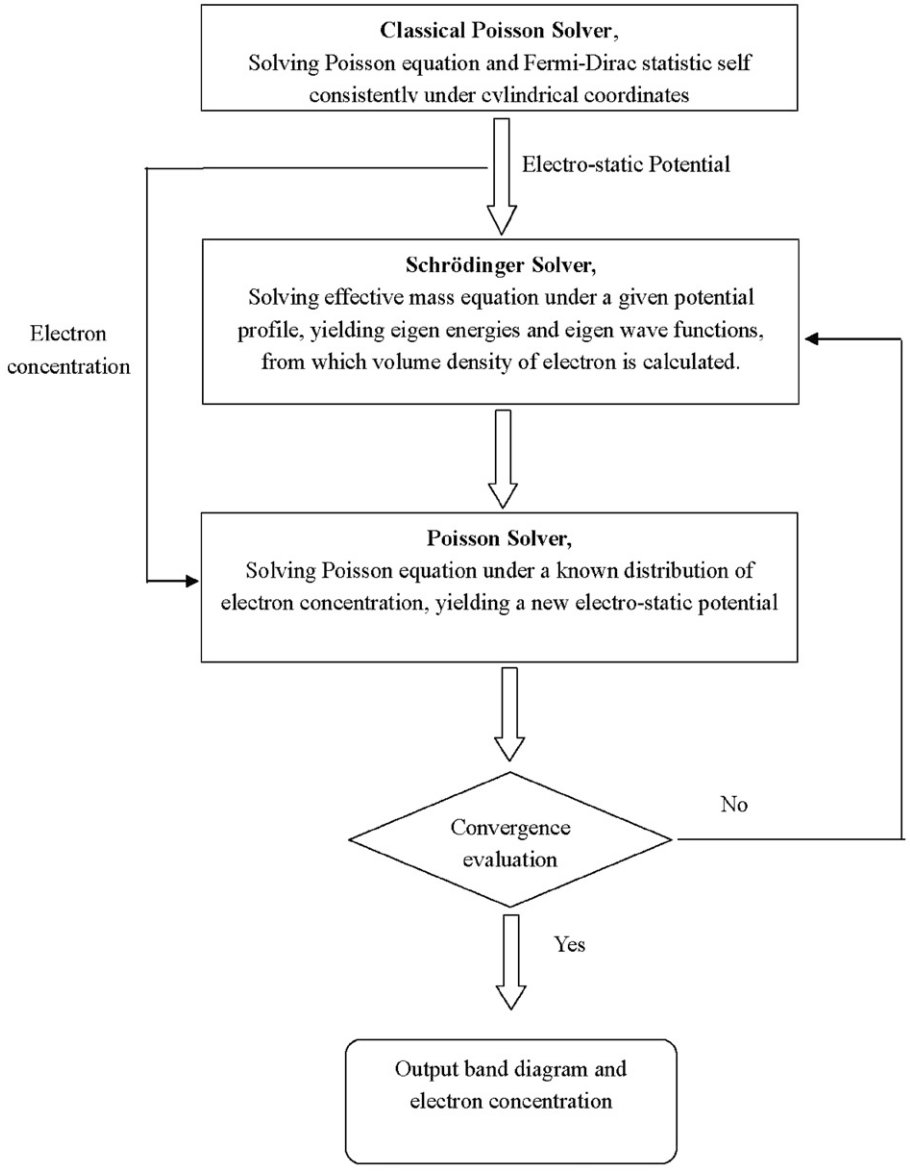

Fig. 2. Flow chart of the self-consistent solution of the Schrödinger equation and the Poisson equation.

as a function of position (where the electron concentration is derived from the Schrödinger solver). Detailed implementation of the individual Poisson solvers are described below.

For the initial guess Poisson solver, the following set of equations is solved self-consistently with a Newton–Ralphson iteration:

$$\left(\frac{d^2}{dr^2}+\frac{1}{r}\frac{d}{dr}\right)\varphi = -\frac{q(N_d^+ - n)}{\varepsilon} \qquad (9)$$
$$n = N_c F_{1/2}(E_c - E_c) \quad \text{while } E_c = -q\varphi + \Delta E_c(r)$$

Here $F_{1/2}(E)$ is the Fermi integral of order $\frac{1}{2}$. N_d^+ is the radial distribution of ionized donors (or acceptors); E_f is the Fermi level, taken to be 0 (it serves as the reference level for energy). The surface boundary condition, i.e. the surface potential, is determined by the externally applied voltage. Interfacial charging at the core–shell boundary could be readily accounted for by adding the potential contribution due to the interfacial charge. If cylindrical symmetry is assumed, and also the energy-wise distribution of surface states is known, an extra potential with the form $\varphi' = -\frac{\sigma}{\varepsilon} r_{core} \ln\frac{r}{r_{core}}$ should be included for $r > r_{core}$ (within the shell region), σ here is the interfacial charge density per unit area.

The second Poisson solver calculates the potential distribution with a known electron distribution. In order to improve the numerical stability, the differential equation is converted into an integral equation. We denote by $\delta\phi$ the difference between the potential profile of two consecutive iterations, and by δn the difference between the electron concentrations as a function of position in successive iterations. The equivalent Poisson equation is written as

$$\left(\frac{d^2}{dr^2}+\frac{1}{r}\frac{d}{dr}\right)\delta\varphi = \frac{q\,\delta n}{\varepsilon} \qquad (10)$$

Integrating the above equation once, results in the following:

$$\frac{d(\delta\varphi)}{dr} = \left.\frac{d(\delta\varphi)}{dr}\right|_{r=0} + \frac{1}{r}\int_0^r \frac{q(\delta n)}{\varepsilon}\,dr' \qquad (11)$$

As a result of symmetry, the electric field at the center is zero, i.e. $\delta\phi'|_{r=0} = 0$. With a second integration, the expression for $\delta\phi$ becomes

$$\delta\varphi = \int_0^r \frac{dr'}{r'}\int_0^{r'} \frac{q(\delta n)}{\varepsilon}\,dr'' + C \qquad (12)$$

If the surface potential is known and fixed (by means of applying a fixed gate bias or Fermi pinning), then $\delta\phi|_{r=r_{max}} = 0$, by which the constant C can be specified.

2.3. Self-consistent calculation

The self-consistent calculation is carried out as described in the flow chart shown in Fig. 2. An initial solution of the classical Poisson equation in conjunction with the Fermi–Dirac distribution is fed into the Schrödinger solver. Subsequently the calculated wave functions and electron concentration as a function of position are provided to the Poisson solver, from which a new electro-static potential is calculated. The new electro-static potential is compared with the previous one; if it satisfies the convergence criteria, then the calculation is terminated. If not, the new potential is again fed into the Schrödinger solver, and the process is iterated until convergence is reached.

In representative cases, a radial grid with 100–200 equally spaced grid points was established. Convergence could be established with 10–30 iterations. Calculations were carried out on a desktop computer.

3. Model verification

3.1. Infinite cylindrical square potential well

The Schrödinger solver was tested under a specific model potential where exact solutions were known as *J*-type Bessel functions of various orders. The potential was set to be zero inside the core, and infinite in the shell region, which is referred to here as the infinite cylindrical constant potential well. Contributions to the potential from the electron concentration are ignored. The corresponding eigenwave vector values are determined analytically via

$$k_n \cdot r = z_n \qquad (13)$$

where z_n represents the nth root of the *J*-type Bessel function. Eigenenergies were subsequently determined with the knowledge of eigenwave vectors by

$$E_n = \frac{\hbar^2 k_n^2}{2m^*} \qquad (14)$$

Shown in Fig. 3 is the comparison between numerical and analytical even parity wave functions, while the inset tabulates the eigenenergies obtained from both methods. Excellent agreement was observed in this case for the numerical solution and the analytical solution.

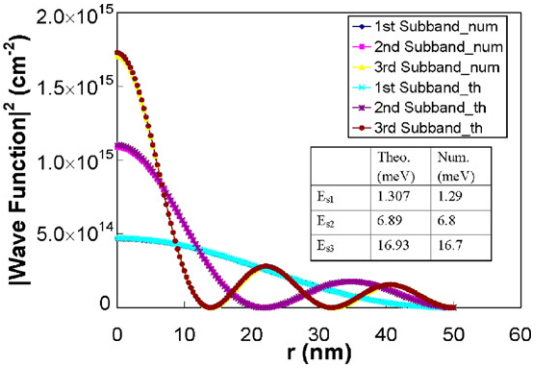

Fig. 3. Model verification for the Schrödinger solver for the case of infinite depth cylindrical potential well. Plotted in the figure are the first three wave functions of even parity, from both numerical calculations and analytical predictions. The inset tabulates the comparison between the eigenenergies obtained from the two methods.

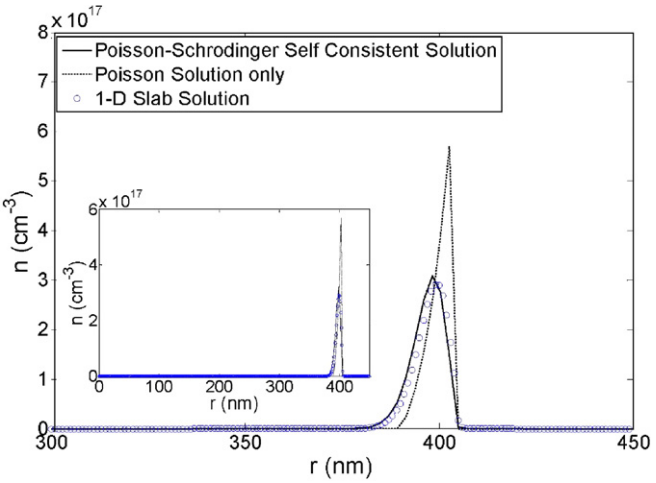

Fig. 4. Model verification by comparing the present solver with a 1D Schrödinger–Poisson slab quantum well solver for a large radius nanowire. The simulation was conducted for a 450 nm radius core–shell structure. The same thicknesses were used in the slab quantum-well solver. Inset shows a comparison within the entire radius range, showing good agreement between the two solutions.

3.2. Comparison with 1D Schrödinger–Poisson solver

To verify the entire self-consistent scheme, we further examined our model in comparison with a well-known 1D Schrödinger–Poisson solver [7]. Although this solver was designed for slab structures, when the core–shell nanowire structure has sufficiently large radius, it should approach the slab case limit. The device dimensions were chosen to be 0.405 μm as the core radius and 0.045 μm as the shell thickness. The simulated temperature was set to be 25 K, to avoid excessive influence from the thermal voltage yet still be able to capture the physical essence of the problem. The comparison between our solution and the 1D solution (with slab thickness set to be equal to the radius) is shown in Fig. 4. Also shown in a dashed line is the classical solution of the Poisson equation only. Good agreement was demonstrated, with a less than 3% mismatch between the two solutions. The difference we believe is due to the equation form itself, i.e. in cylindrical coordinates, the Laplacian operator gives an additional $\frac{1}{r}\frac{d}{dr}$ term, which is a slowly decaying term and still contributes to the wave functions at the radius considered in the given example.

4. Model application

Core–shell nanowire structures are of substantial interest for electrical and optoelectronic applications. Core–shell configurations can utilize a great diversity of semiconductor combinations, since the nanowires are relatively tolerant to lattice mismatch between materials, and the associated stress and strain fields. Quantitative understanding of electron concentrations is important for further work, particularly for the two-dimensional electron gas established at the interface between semiconducting materials in appropriately designed nanowires. We therefore applied our model to a representative device of this type. Shown in Fig. 5 are the computed results for an InAs/GaAs core shell structure, where the inner core is formed of InAs (with radius 36 nm), and the outer shell is of GaAs (so that the overall radius is 40 nm). Bandgap energies and electron masses were taken from [9]. It was assumed that there were no interface states at the boundaries of the materials, and that the band offset in the conduction band corresponds to 0.62 eV (which reflects a 58–42% split in conduction band offset and valence band offset [9]). Fig. 5a presents wave functions for the first few subbands for the core–shell structure. It can be noted that there is a set of subbands corresponding to radial variation of the wave function, in a manner that resembles the subband structure of slab quantum well structures. Each of these subbands has a further splitting associated with the angular variation of the wavefunctions. The radial dependence of the wave functions varies slightly with the angular quantum number, as shown in Fig. 5a. Inasmuch as the externally applied potential has circular symmetry, we can label each subband with s, p, d, ... following the well-established convention. Differences between the radial wave functions due to the angular variation are more pronounced for the higher energy subbands. To illustrate, first few eigenenergies are shown with thinner lines in Fig. 5(b).

The conduction band profile and the electron concentration are shown in Fig. 5(b) and (c), respectively. It is observed that although the conduction band for the quantum wire is below the classically predicted value (which is based on 3-D bulk statistics), the electron density is much smaller near the surface, due to the form of the low energy wave functions and smaller density of states in the 1-D system. Also shown in Fig. 5(b) is the result obtained from the 1D Schrödinger–Poisson slab solver, in which the slab thickness was set to be equal to the radius. Compared to its slab counterpart, the cylindrical solution exhibits more quantum-like corrections, i.e. the peak of the electron concentration is pushed more towards the center, and the concentration peaks at a lower value. Characteristics of quantum-wires with different radius can differ significantly. Shown in Fig. 6 are the conduction band profile and electron concentration as functions of position in a smaller device featuring 20 nm radius (but otherwise identical characteristics to the device in Fig. 5). In the smaller size device, with the same surface potential, the electron density throughout the volume is significantly larger than the 40 nm radius case (which compares well with the known results of increasing volume inversion with thinner slabs in the slab-like FinFET devices [10]).

The general-purpose Schrödinger–Poisson solver described here can be used in various nanowire device contexts. The numerical solver provides the capability to find discrete eigenenergies, identify corresponding wave functions, specify the electron concentration as a function of

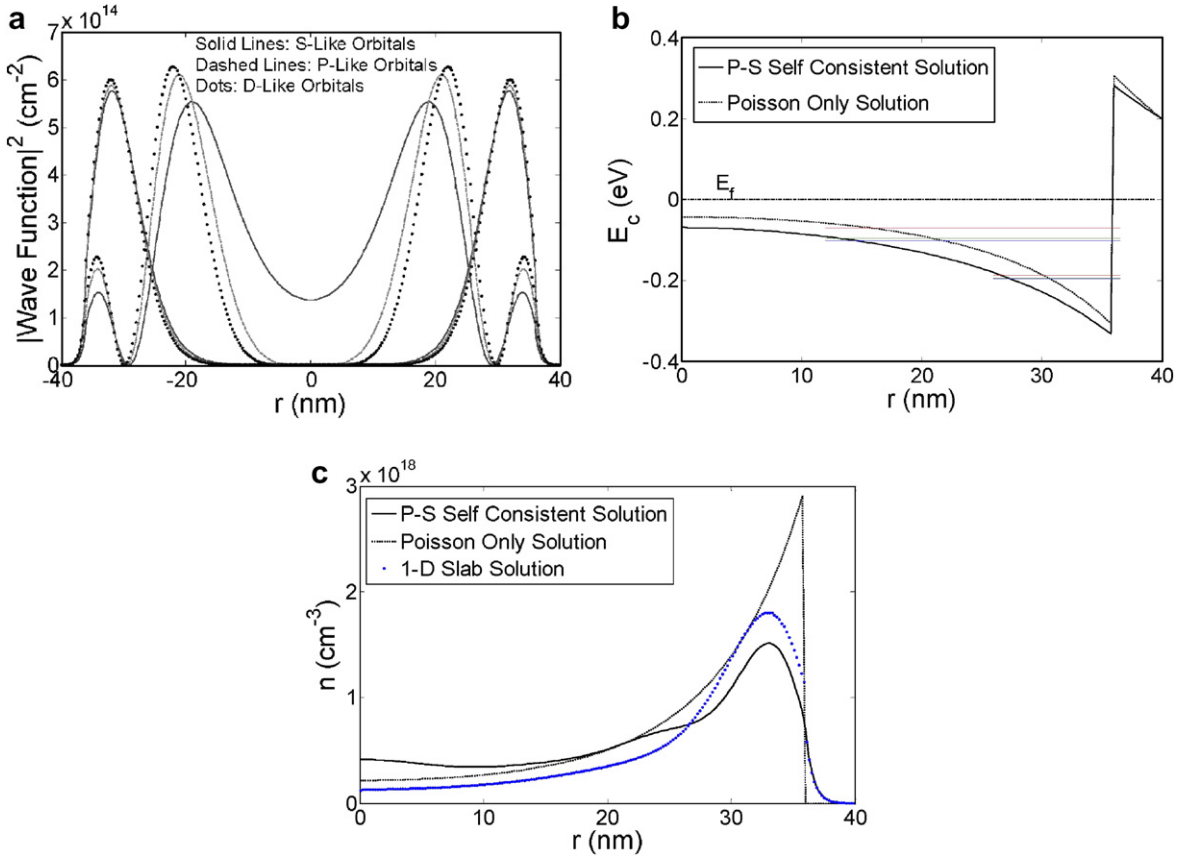

Fig. 5. Model application to the self-consistent calculation of 2-DEG formation in an InAs/GaAs core shell structure. The calculated structure has an overall radius of 40 nm; the InAs core radius is 36 nm. (a) Wave functions for first few subbands. (b) Conduction-band energy for the quantum self-consistent solution (solid line) and classical Poisson only solution (dashed line). Eigenenergies were also shown with thin lines, corresponding to the wave functions shown in (a). (c) Electron distribution in quantum self-consistent solution (solid line) and classical Poisson only solution (dashed line). Also provided is the solution from the slab quantum-well solver for a slab sandwich structure constituted by InAs and GaAs with thicknesses as 36 nm and 4 nm.

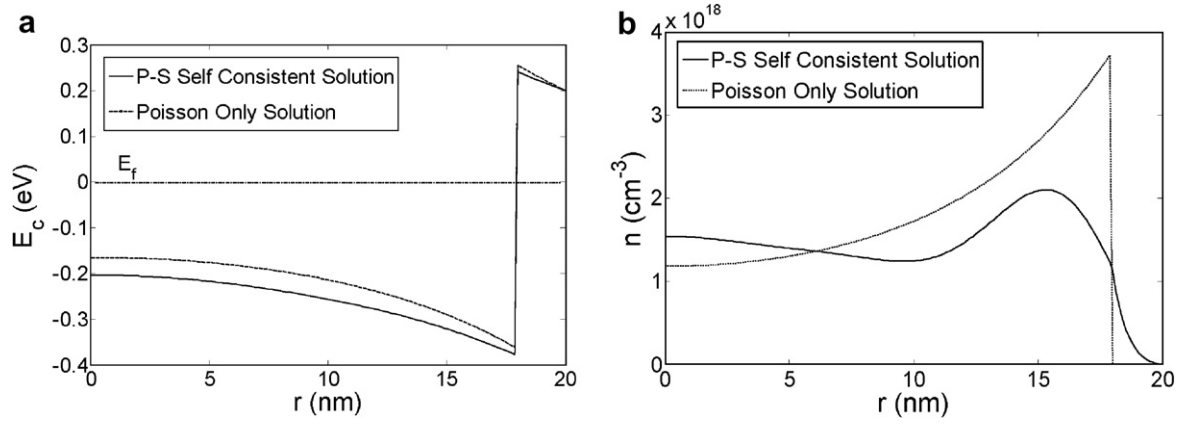

Fig. 6. Model application to the self-consistent calculation of 2-DEG formation in an InAs/GaAs core shell structure. The calculated structure has an overall radius of 20 nm; the InAs core radius is 18 nm. The results show a more pronounced volume electron density than in the case of Fig. 5.

position, and calculate electrostatic potential and radial electric fields. From these basic functions additional capabilities can be derived, such as calculating the capacitance–voltage characteristics of FET structures. The geometry of a representative nanowire FET, with core–shell structure and metal gate, is shown in Fig. 7a. For simplicity yet without losing any physical essence, we ignored here the contact potential between a metal gate and the shell material. For a

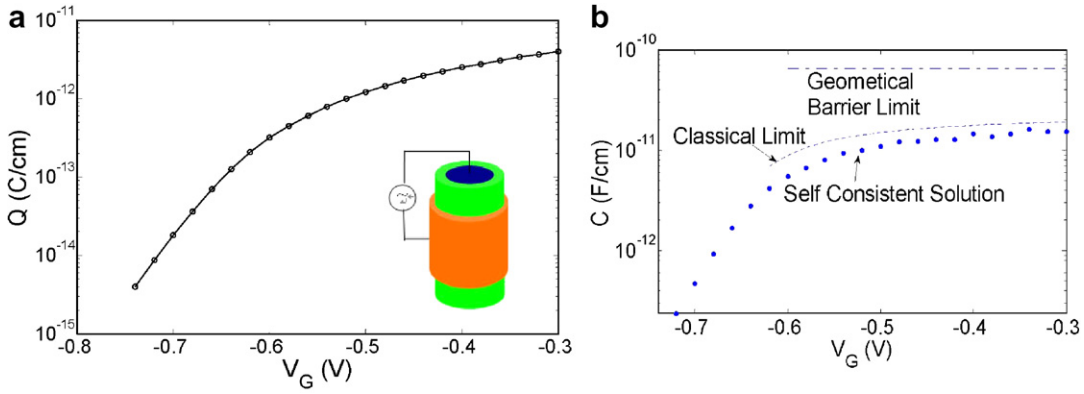

Fig. 7. (a) Predicted Q_s–V characteristic for a structure similar to that of Fig. 5. (b) Derived C–V characteristic for the same structure, with comparison of the classically predicted C–V curve, the horizontal line is the capacitance calculated as a co-axial cylindrical capacitor. Inset of (a) shows schematically the structure under consideration.

given voltage difference between the metal Fermi level and the Fermi level of electrons in the nanowire, the overall charge Q can be calculated, and the C–V curve can be further evaluated through $C = \mathrm{d}Q/\mathrm{d}V$. Fig. 7 is a demonstration of this capability for a 40 nm radius InAs/GaAs core–shell structure with 4 nm thick GaAs barrier layer. Interestingly, the Q–V curves exhibit ideal 60 mV/dec "subthreshold" characteristic, which is expected for the ultra-thin-body fully depleted FET devices. It is noticed that the resulting gate capacitance is considerably lower than its geometrical barrier limit (only ~1/3 the value calculated as a co-axial cylinder capacitor between the gate metal and the InAs/GaAs interface); and is ~70% of the classically predicted capacitance.

The reduction of gate capacitance can be understood via the carrier distribution: self-consistent calculation predicts that the charge centroid is pushed away from the InAs/GaAs interface both classically and, additionally from the quantum effects known as the energy quantization and reduced 1-D density of state (DOS) (see Figs. 5(c) and 6(b)) [11]. The capacitance reduction is considered detrimental in terms of reduced transistor transconductance. To characterize effects from different mechanisms, we employ a phenomenological equivalent circuit depicted in Fig. 8, where the gate capacitance C_g is considered to be a series combination of the classically predicted gate capacitance and a quantum correction capacitance $C_{qc} \cdot C_{qc}$ originates from the finite spread of the wave function

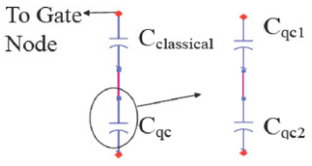

Fig. 8. Equivalent circuit for de-embedding quantum capacitances. C_{qc} is the collective quantum capacitance, while C_{qc1} stands for the influence due to the finite wave function spread; C_{qc2} accounts for the influence due to the reduced DOS.

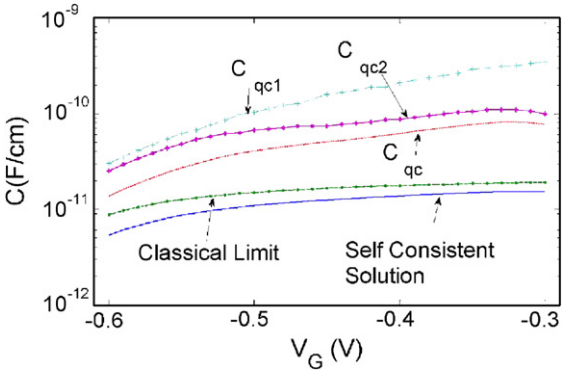

Fig. 9. De-embedded quantum capacitances as functions of voltage.

associated with each energy level and the reduced DOS from the low dimensionality of the structure. To further distinguish the relative importance of these mechanisms, we introduce C_{qc1} and C_{qc2} to account for their individual contributions; the total quantum capacitance C_{qc} is a series combination of C_{qc1} and C_{qc2} (see Fig. 8).

The de-embedding proceeds as following (using results presented in Fig. 7): first, C_{qc} is de-embedded given the classically predicted value and the self-consistent quantum mechanical solution (shown in Fig. 9); second, C_{qc1}, which represents the influence from finite wave function spread, is obtained by substituting the 3-D DOS function into (8) instead of the 1-D DOS function used previously, so that the 1-D DOS influence is excluded; third, with the knowledge of C_{qc} and C_{qc1}, C_{qc2} was calculated via the equivalent circuit presented in Fig. 8. For this particular example, it is shown that the low dimensionality is the dominant mechanism of the reduced gate capacitance.

5. Limitations of the model

Various simplifications have been introduced into the solver which can limit the accuracy in a number of

situations. As noted above, the effective mass is assumed to have a constant value. Thus non-parabolicity effects are not taken into account. The implied isotropy of the effective mass omits a number of details present in the conduction band of Si and other multi-valley semiconductors. Our present treatment of holes is also associated with a simple effective mass; the full complexity of light and heavy hole bands and their interactions are ignored.

6. Summary

A general-purpose Schrödinger–Poisson solver was developed for symmetric structures in cylindrical coordinates. This solver is useful for a wide range of semiconductor nanowire problems. The solver allows evaluation of discrete eigenenergies, and wave functions for a given geometry, based on which the electro-static potential and the electron concentration can be calculated, all in a self-consistent manner. Self-consistent C–V characteristics of a given structure can be readily deduced from the model, and compared to their classical counterparts, which allows for assessment of the impact of quantum capacitance. A de-embedding method is further introduced to distinguish individual contributions from finite wave function spread and low dimensionality to the quantum capacitance.

References

[1] Huang Y, Lieber CM. Integrated nanoscale electronics and opto-electronics: exploring nanoscale science and technology through semiconductor nanowires. Pure Appl Chem 2004;76:2051–68.
[2] Hahm J, Lieber CM. Direct ultrasensitive electrical detection of DNA and DNA sequence variations using nanowire nanosensors. Nano Lett 2004;4:51–4.
[3] Gu Y, Kwak E-S, Lensch JL, Allen JE, Odom TW, Lauhon LJ. Near-field scanning photocurrent microscopy of a nanowire photodetector. Appl Phys Lett 2005;87:043111 [cover article].
[4] Duan X, Huang Y, Agarwal R, Lieber CM. Single-nanowire electrically driven lasers. Nature 2003;421:241–5.
[5] Cui Y, Zhong Z, Wang D, Wang WU, Lieber CM. High performance silicon nanowire field effect transistors. Nano Lett 2003;3:149–52.
[6] Bryllert T, Samuelson L, Jensen L, Wernersson L. Vertical high mobility wrap-gated InAs nanowire transistor. In: DRC proceedings, 2005, p. 157–8.
[7] Tan I-H, Snider GL, Chang LD, Hu EL. A self-consistent solution of Schrödinger–Poisson equations using a nonuniform mesh. J Appl Phys 1990;68(8):4071–6.
[8] http://mathworld.wolfram.com/BesselFunctionoftheFirstKind.html.
[9] Sze SM. Physics of semiconductor devices. 2nd ed. John Wiley & Sons; 1981 [Appendix G].
[10] Brübach J, Silov AYu, Haverkort JEM, Vleuten Wvd, Wolter JH. Coupling of ultrathin InAs layers as a tool for band-offset determination. Phys Rev B 1999;59(15):10315–26.
[11] Lopez-Villanueva JA, Cartujo-Cassinello P, Gamiz F, Banqueri J, Palma AJ. Effects of the inversion-layer centroid on the performance of double-gate MOSFETs. IEEE Trans Electron Dev 2000;47(1):141–6.